

## **Effect of Nano BaTiO<sub>3</sub> Particles on Properties of Semi-IPN System Prepared from Polyetherimide and biscitraconimide**

Preshi Gupta\*, Rakesh Kumar Gupta and Sarfaraz Alam

Defence Materials and Stores Research and Development Establishment, DMSRDE Post  
Office, G. T. Road, Kanpur-208013, India.

---

### **Abstract**

Polyetherimide/biscitraconimide/BaTiO<sub>3</sub> nanocomposite films were prepared by mixing BaTiO<sub>3</sub> nanoparticles into Polyetherimide/biscitraconamic acid solution under sonication followed by film casting and thermal imidization. Fourier transform infrared (FTIR), X-Ray Diffraction (XRD) and Scanning Electron Microscopy (SEM) techniques were used to characterize the structure and properties of obtained nanocomposites. Thermal performance of nanocomposites was determined by Differential Scanning Calorimetry (DSC) and Thermo Gravimetric Analysis (TGA). It was found that thermal stability of nanocomposites was increased with increasing concentration of BaTiO<sub>3</sub> nanoparticles. The dielectric properties of nanocomposite films were discussed for various filler contents. The dielectric constant ( $\epsilon$ ) of these nanocomposites increased with increase in the weight percent of BaTiO<sub>3</sub> nanoparticles.

**Key words:** BaTiO<sub>3</sub> nanoparticles, semi-2-IPNs, PEI, biscitraconimide, bis(3-aminopropyl)phenyl phosphine.

---

Date of Submission: 21-02-2021

Date of acceptance: 04-03-2021

---

### **I. INTRODUCTION**

Composite consisting of a polymer matrix and dispersed ceramic particles is a kind of material with great potential properties and applications. By integrating the advantages of two phases, the composite materials can offer enhanced performances far beyond those of the individual constituent materials [1, 2]. In addition, their properties can be designed according to specific requirements by changing the fraction of the constituents. Therefore construction of organic–inorganic composites has attracted considerable attention in many applications, such as packaging material, circuit board, interlayer dielectrics, antenna, and passive protection. Polymers possess limitations for much higher performance applications in which inorganic materials are used, because of their intrinsic nature as organic materials. Inorganic materials exhibit excellent thermal stability and functional properties such as dielectric and magnetic properties, but high brittleness and bad film forming characteristics. Thus, the composite formation of polymers with inorganic material has been suggested to meet the demands of balanced properties for both organic and inorganic materials [3, 4]. The overall properties of a composite material can be determined not only by the properties of the parent components but also by the morphology, volume fractions, and connectivity of the phases as well as their interfacial properties [5, 6]. A number of methods such as solution mixing, melt blending and insitu polymerization for preparing polyimide nanocomposites have been reported [7]. A wide range of organic–inorganic composites could be prepared by the appropriate selection of the raw materials and preparative approaches, in order to make finely dispersed particles in polymer matrix while minimizing agglomeration, and to obtain properties to meet the requirements of different applications [8, 9].

Varieties of ceramic polymer composites have been investigated to enhance certain performances, including the dielectric properties. Barium titanate (BaTiO<sub>3</sub>) is one of the most used ferroelectric ceramic because of its high dielectric constant as well as unique piezoelectric and pyroelectric properties. Possessing very high dielectric constant, barium titanate based ceramic has been widely utilized as capacitors and piezoelectric transducers. In order to minimize the size of the capacitor and electronic components, recent attempts are mainly focused on fabricating BaTiO<sub>3</sub> films with thin thickness, high dielectric constant and processing easiness however reducing the thickness of the film is fundamentally limited by the brittle nature of BaTiO<sub>3</sub>.

\*Corresponding author: Email: [preshigupta4@gmail.com](mailto:preshigupta4@gmail.com), Tel: +91-5122451759-78, Fax: +91-5122450404

Among the polymers, polyimides (PI) possess reliable high temperature stability, good mechanical strength and excellent chemical resistance. In recent years, the preparation of polyimide composite materials has been extensively studied due to the dramatic improvements over their pure state in the thermal stability, mechanical properties and other functional features by introducing only small fraction of inorganic fillers [10-13]

But a single polymeric material suitable as a matrix for the fabrication of composites that has both toughness and good compressive modulus has not been found. Polymeric matrix resins that have good compressive modulus generally possess high cross-link density which imparts brittleness. On the other hand, tough resins have poor processability because of their very high melt viscosity at the processing temperature. Thus to overcome the above disadvantages the concept of semi-interpenetrating polymeric networks (semi-IPNs) has been developed to obtain macromolecular systems which combine the high temperature properties of thermoplastic polymers and processability of thermosetting polymers [14-18]. Semi-IPNs are composed of two chemically different polymers, one is crosslinked and the other is linear.

Therefore, different compositions of semi-IPN polyimide system were prepared through solution blending using biscitraconimide (MBMI) and polyetherimide (PEI) as previously reported [19]. Since PEI (Figure 1) is an excellent engineering thermoplastic having good mechanical properties as well as high glass transition temperature (T<sub>g</sub>) and thermo-oxidative stability. Whereas phosphorous containing biscitraconimide resin was prepared by reacting citraconic anhydride (CA), 3,3',4,4'-benzophenone tetracarboxylic dianhydride (BTDA) and bis(3-amino propyl)phenyl phosphine (BAPPP). One important advantage of phosphorous containing polyimide is that these resins show good flame resistant properties. The synergistic fire retarding properties of phosphorous and nitrogen containing functionalities are well documented in literature [20]. Moreover incorporation of flexible chain segment helps to overcome brittleness and enhance ductility as well as toughness [21]. Among them 20:80 MBMI: PEI composition was chosen for composite fabrication due to its flexible film forming ability with maximum thermoset fraction coupled with good optical transparency and flame retardant property.

Only a few researchers have studied the synthesis and characterization of polyimide/BaTiO<sub>3</sub> nanocomposites. So far, to the best of our knowledge, preparation of polyimide semi-IPN based nanocomposites has not been found. Thus in the present study polyimide semi-IPN based nanocomposites films were prepared by using PEI/biscitraconamic acid precursor solution and BaTiO<sub>3</sub> nanoparticles via in-situ polymerization method. Here biscitraconamic acid was used as a precursor of biscitraconimide (MBMI). The semi-IPN nanocomposites films were examined for their spectral, thermal, morphological and electrical properties.

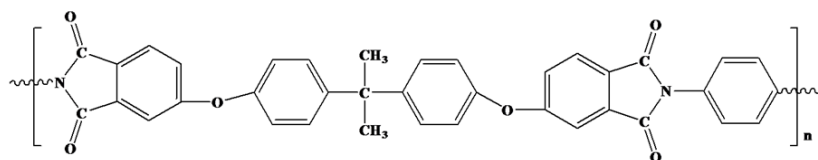


Figure 1: Chemical structure of PEI.

## II. EXPERIMENTAL

### 2.1: Materials

Barium acetate and Titanium isopropoxide (Acros Organics, New Jersey, USA) Glycerol (Qualigens, Mumbai, India) and Acetic acid (Samir Tech Pvt. Ltd., Vadodra, India) were used as received. Polyetherimide (Ultem® 1000) was supplied by General Electric Plastics, USA in pellet form and was dried for 8 h in an oven at 150°C before use to remove moisture, if any. Bis(3-aminopropyl)phenyl phosphine (Alfa Aesar) and citraconic anhydride (Aldrich) was used as received. 3,3',4,4'-benzophenone tetracarboxylic dianhydride supplied by Aldrich was recrystallized from acetic anhydride before use. N,N-dimethylacetamide (DMAc) from Merck was purified by distillation over phosphorous pentoxide under reduced pressure and stored over 4Å molecular sieves.

### 2.2: Measurements

The infrared spectra were recorded on the Perkin Elmer FTIR spectrophotometer (Model RX1) using KBr pellets in the range 4000-400 cm<sup>-1</sup>. Glass transition temperature (T<sub>g</sub>) was determined by differential scanning calorimetry (DSC), Model DSC Q 200, TA instruments; USA at a heating rate of 10°C/min under nitrogen atmosphere at a flow rate of 50ml/min. Degradation temperatures were recorded by Hi-Res TGA 2950 thermogravimetric Analyzer (TA instruments), at a heating rate of 10°C/min under nitrogen atmosphere. About 7±2 mg of sample was heated at 10°C/min from room temperature to 1000°C in a dynamic nitrogen atmosphere (flow rate 60ml/min). X-Ray diffractograms (XRD) were recorded on an ARL XTRA X-ray diffractometer

(Thermo Electron Corporation) with CuK $\alpha$  radiation in the 2 $\theta$  range from 20° to 80°, by a step of 0.02°. The particle size distribution and morphology was determined by Carl-Zeiss EVO 50 Low Vacuum scanning electron microscope (LVSEM) at acceleration of 20 kV. The dielectric properties of the films were characterized using Aligent 4294 Precision Impedance Analyzer at frequencies of 10 KHz, 100 KHz and 1 MHz. The moisture permeation of the composite films was evaluated using a water absorption test. The dried composite films were subjected to immersion in water for 48h to ensure saturation. Water absorption was calculated according to the percentage of weight gained after the immersion.

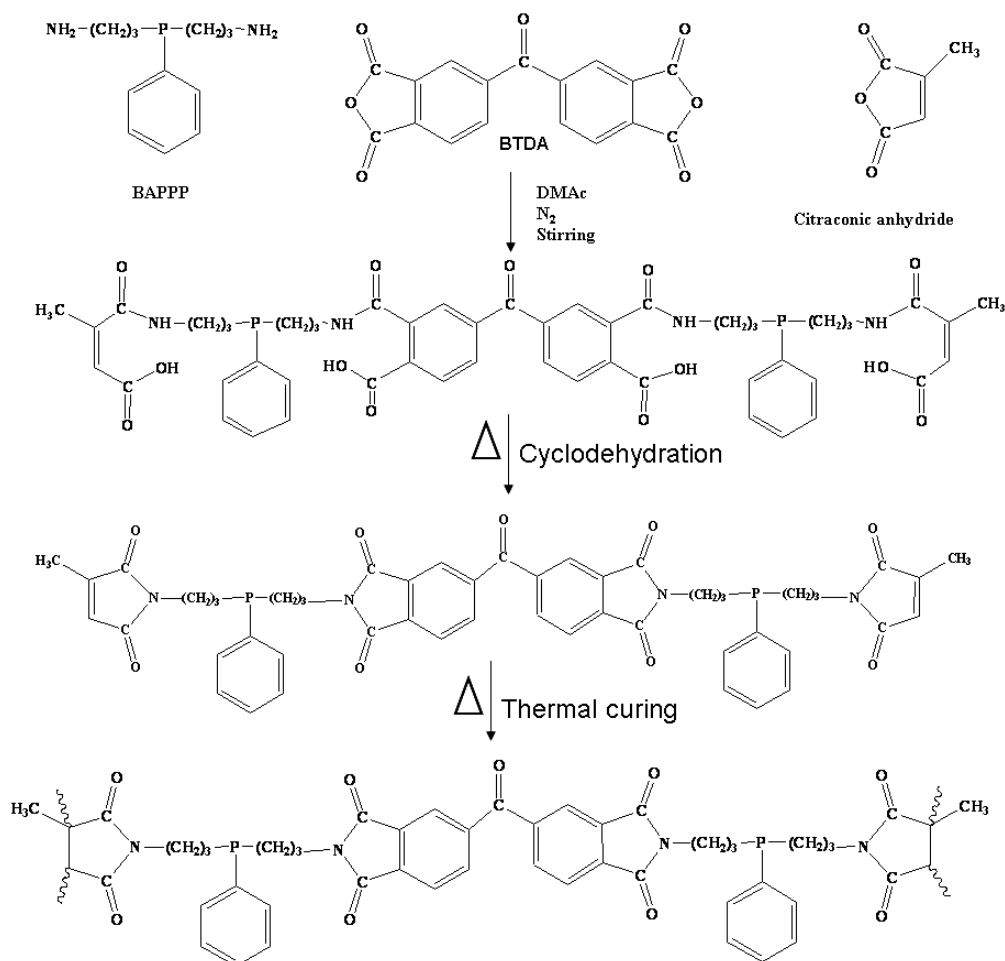
### **2.3: Synthesis of BaTiO<sub>3</sub> nanoparticles**

BaTiO<sub>3</sub> nanoparticles were synthesized in our laboratory by Sol-Gel technique [22]. In this process, titanium isopropoxide and barium acetate in the molar ratio of 1:1 were taken in distilled water. Then it was stirred continuously for 8 hrs at room temperature. During the stirring a few drops of acetic acid and glycerin were added to avoid precipitation. Thereafter, the solution was dried at 100°C for 24h to form gel. Annealing of this gel was done at 850°C for 2h in an electrically heated refractory high temperature furnace to produce BaTiO<sub>3</sub> nanoparticles.

### **2.4: Synthesis of Biscitraconamic acid**

Biscitraconamic acid (CA/BAPPP/BTDA), the chemical structure of which is shown in Scheme 1, was prepared in two steps. Step one concerns the reaction of diamine and dianhydride (BAPPP/BTDA). Step two deals with the addition of citraconic anhydride with BAPPP/BTDA according to the following procedure.

A 500 ml three neck round bottom flask equipped with a nitrogen inlet, a stir bar and a guard tube was charged with 41.67 mmol of diamine (BAPPP) and 150 ml of freshly distilled DMAc. The solution was stirred until the diamine dissolved completely. 20.84 mmol of dianhydride (BTDA) was added in fractions to this solution under effective stirring. The reaction mixture was stirred for 8h at room temperature. A solution of 41.67 mmol of citraconic anhydride (CA) in 50 ml DMAc was added to the same solution over a period of 15 minutes. After 10 minutes the colour of the reaction changes from white to yellow, room temperature stirring for 8h was further continued to ensure complete reaction. DMAc was distilled under reduced pressure (10mm of Hg) at 90°C, the solid material obtained was biscitraconamic acid (MW 922 gm/mole). After that dry benzene was added to biscitraconamic acid and further distilled. This process was repeated twice in order to remove moisture completely. Biscitraconamic acid was obtained in quantitative yield.



Scheme 1: Schematic of crosslinked biscitraconimide synthesis route.

### 2.5 Synthesis of PEI/MBMI semi-IPN/ BaTiO<sub>3</sub> nanocomposite films

BaTiO<sub>3</sub> nanoparticles (1 wt%) was added into DMAc solvent and ultrasonicated for 4h. For preparing semi-IPN system, 1.085 ml (217mg), 20 wt% solution of biscitraconamic acid (equivalent to 200 mg of biscitraconimide, mol. wt. 850) in DMAc was mixed with 4 ml (800 mg) 20 wt% solution of PEI in the same solvent. The mixture was stirred for 1h at room temperature to give a clear brown solution, which contained 20% by weight of solid. The weight ratio of biscitraconimide and PEI was 20 to 80 and this composition was designated as PM. Then the above BaTiO<sub>3</sub> suspension was added to PEI/biscitraconamic acid solution and the reaction mixture was ultrasonicated for another 4h at room temperature in order to ensure fine dispersion of BaTiO<sub>3</sub> nanoparticles in PEI/MBMI semi-IPN matrix. Then the reaction mixture was poured on a clean and dry glass plate and thermal imidization was carried out in an oven at 100 and 150°C for 2h at each temperature then 200, 250 and 300°C for 1h at each temperature. Other compositions of nanocomposites were prepared in similar manner by adding the above components in the required ratios and their formulations are given in Table 1.

Table 1: Sample Codes for PEI/MBMI semi-IPN and PEI/MBMI/BaTiO<sub>3</sub> nanocomposites.

Sample Code	PEI (wt %)	MBMI (wt %)	BaTiO <sub>3</sub> Nanoparticles (wt %)
PM	80	20	-----
PM1	80	20	1
PM2	80	20	2
PM3	80	20	3
PM4	80	20	4
PM5	80	20	5

## III. RESULT AND DISCUSSION:

### 3.1: FT-Infrared Spectroscopy

The FTIR spectra of pure BaTiO<sub>3</sub>, PEI/MBMI Semi-IPN polyimide matrix and their nanocomposites are shown in Figure 2. The FTIR absorption spectrum of pure BaTiO<sub>3</sub> demonstrates two broad characteristic

absorption peaks at 560 and 450 cm<sup>-1</sup> due to Ti-O stretching and bending vibrations [23, 24]. IR spectroscopy is a useful tool for qualitative assessment of the imidization process. The spectrum of PEI/MBMI semi-IPN shows characteristic imide group absorptions at 1780 and 1720 cm<sup>-1</sup> (asymmetrical and symmetrical stretching of imide carbonyl bond), 1380 and 735 cm<sup>-1</sup> (C-N stretching and bending) [20].

Similar absorption bands are also observed in PEI/MBMI/BaTiO<sub>3</sub> nanocomposites as shown in Figure 2(c). These results clearly confirmed the complete imidization of amic acid into imide in PEI/MBMI/BaTiO<sub>3</sub> nanocomposites. The characteristic absorption peaks due to both PEI/MBMI semi-IPN and BaTiO<sub>3</sub> are observed in nanocomposite. The peak positions of the absorption bands for each component are remaining almost unchanged in nanocomposite when compared with the IR spectra of pure BaTiO<sub>3</sub> and PEI/MBMI semi-IPN system. This result revealed the success of synthesizing the PEI/MBMI/ BaTiO<sub>3</sub> nanocomposites.

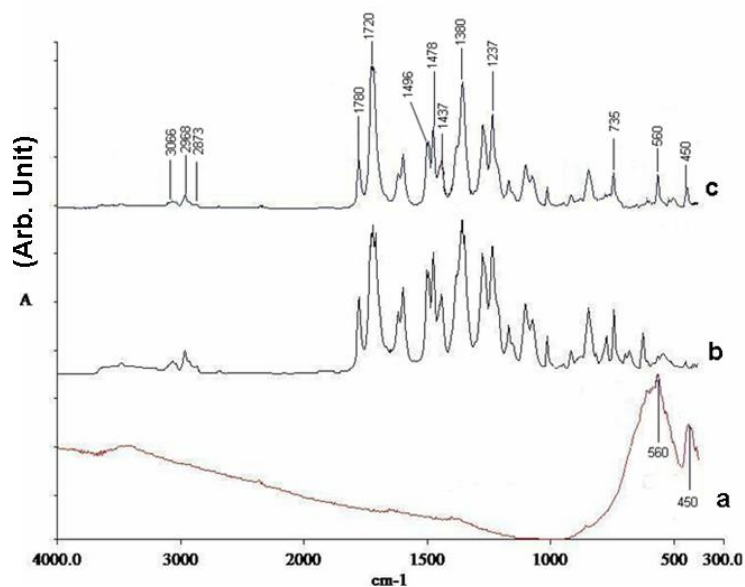


Figure 2: FTIR spectra of (a) BaTiO<sub>3</sub> nanoparticles (b) PEI/MBMI semi-IPN (c) PEI/MBMI/ BaTiO<sub>3</sub> nanocomposite.

### 3.2: X-Ray Diffraction

XRD diffractograms of BaTiO<sub>3</sub>, PEI/MBMI/ BaTiO<sub>3</sub> nanocomposite are shown in Figure 3 (a, and b). The diffraction peaks in Figure 3(a) are in accordance with the standard peaks for cubic barium titanate based on the JCPDS card 31-0174. The crystal size was calculated using the Scherrer equation:

$$d = \frac{k\lambda}{\beta \cos\theta} \dots\dots\dots\text{Eq 1}$$

Where, d is the primary particle size; k is the Scherrer constant (0.889), λ is the wavelength of CuKα radiation (1.5405 Å), θ is the diffraction angle and β is the Full Width of Half Maxima (FWHM) of the peak. The average size of the particles calculated is 30 nm. The XRD pattern in Figure 2(b) confirms the incorporation of BaTiO<sub>3</sub> as almost all characteristic peaks of BaTiO<sub>3</sub> at 31.14, 38.37, 45.63, 51.07, 55.46, 65.32 2θ are present in nanocomposite also.

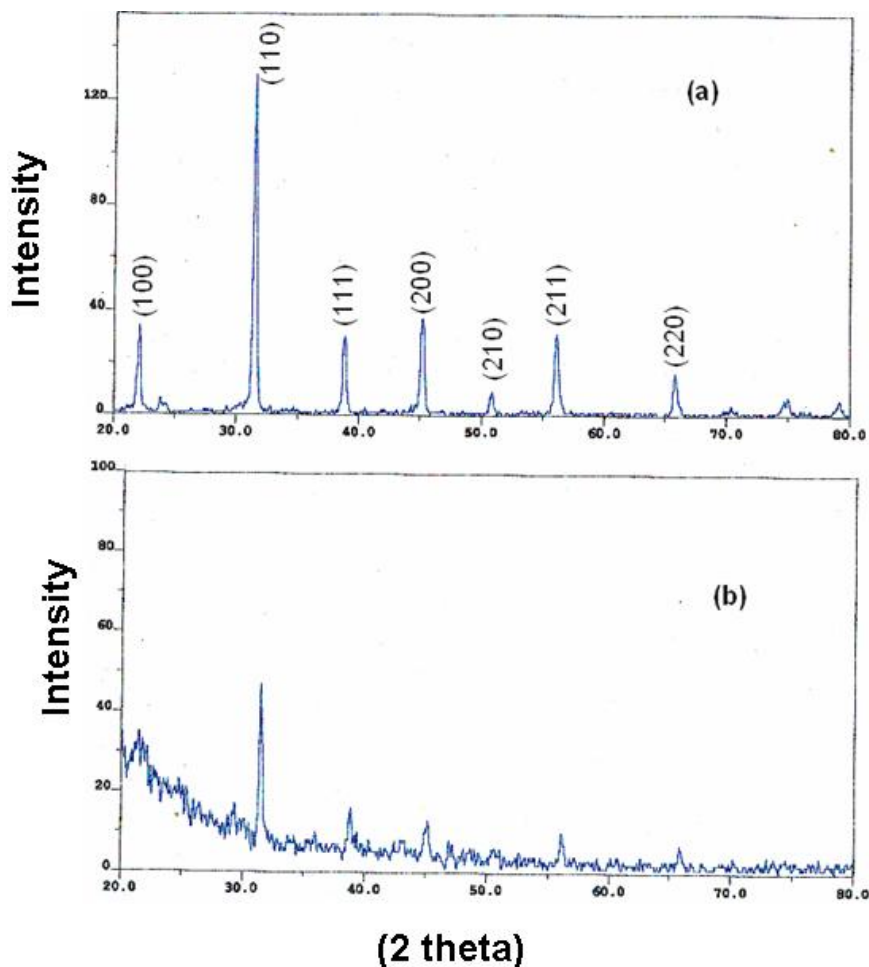


Figure 3: XRD spectra of (a) BaTiO<sub>3</sub> (b) PEI/MBMI/ BaTiO<sub>3</sub> nanocomposite.

### 3.3: Thermal studies

Thermal studies of nanocomposites were carried out by Differential Scanning Calorimetry (DSC) and Thermo Gravimetric Analysis (TGA).

#### 3.3.1: Differential Scanning Calorimetry (DSC)

The thermal behavior of PEI/MBMI/BaTiO<sub>3</sub> nanocomposites was evaluated by DSC. DSC measurements were conducted at a heating rate of 10°C/min under nitrogen atmosphere. Samples were dried at 150°C for 5h in an oven before DSC measurement in order to remove residual solvent and moisture which may influence their glass transition temperature ( $T_g$ ). Table II summarizes the thermal data of neat PEI/MBMI semi-IPN system and different compositions of PEI/MBMI/BaTiO<sub>3</sub> nanocomposites. From Figure 4 it is clear that the  $T_g$  shows upward shift with increase in the wt% of BaTiO<sub>3</sub>. It may be due to ionic groups present on the surface of BT nanoparticles, which interact and modify the intermolecular forces, thus hindering the segmental mobility of the semi-IPN chains. This results in an increase in  $T_g$  of the nanocomposites [25, 26].

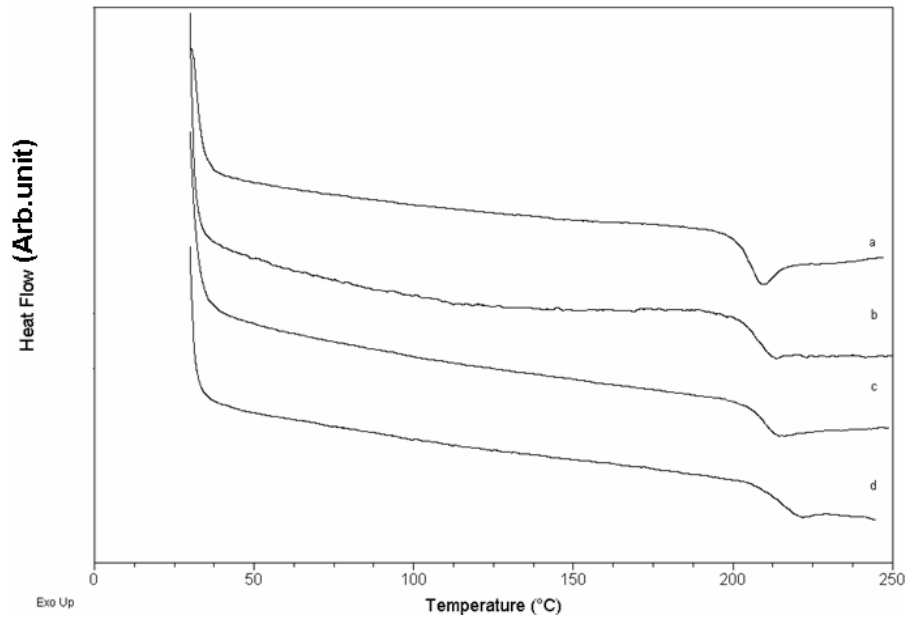


Figure 4: DSC curves of (a) PEI/MBMI semi-IPN (b) PM1 (c) PM3 (d) PM5.

### 3.3.2: Thermo Gravimetric Analysis

To investigate the effect of BaTiO<sub>3</sub> incorporation on the thermal stability of PEI/MBMI semi-IPN system, TGA was performed. Figure 5 shows the TGA weight loss curves for semi-IPN system and nanocomposites in nitrogen atmosphere. All the nanocomposites showed higher thermal stability as compared to the parent matrix. The onset degradation temperature of PEI/MBMI semi-IPN system was found to be 435°C which increases to 436, 440 and 444°C with incorporation of 1, 3 and 5 wt% of BaTiO<sub>3</sub> nanoparticles. The reason can be explained as; incorporation of BaTiO<sub>3</sub> nanoparticles reduces the chain mobility of the polymer matrix by imposing vast numbers of restriction sites which reduces the thermal vibration of the C–C bonds [27]. So the nanocomposites require more thermal energy for the degradation of the polymer matrix which in turn increases their thermal stability.

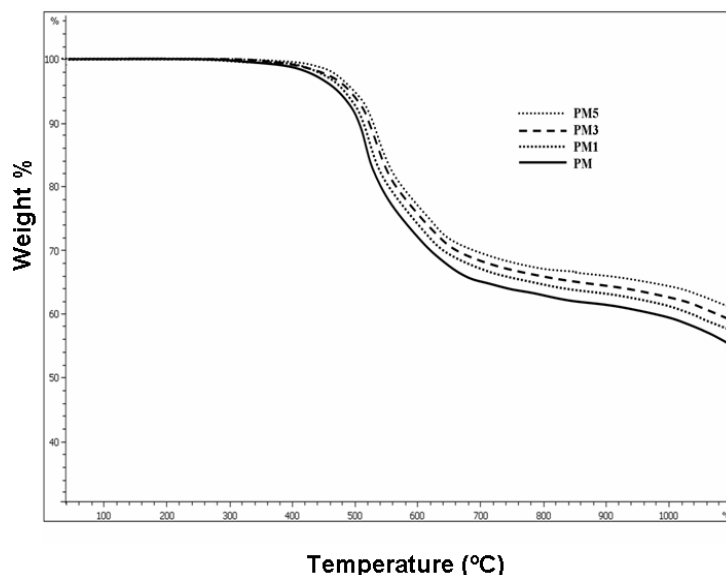


Figure 5: TGA thermographs of (a) PEI/MBMI semi-IPN (b) PM1 (c) PM3 (d) PM5.

**Table 2: Thermal data of PEI/MBMI semi-IPN system and various compositions of PEI/MBMI/BaTiO<sub>3</sub> nanocomposites.**

Sample designation	T <sub>g</sub> <sup>a</sup> (°C)	T <sub>i</sub> <sup>b</sup> (°C)	T <sub>max</sub> <sup>c</sup> (°C)	T <sub>f</sub> <sup>d</sup> (°C)	Y <sub>c</sub> <sup>e</sup> (% at 800°C)
PM	209	435	513	646	64
PM1	210	436	514	647	65
PM2	211	439	516	649	66
PM3	212	440	517	651	67
PM4	213	443	519	653	68
PM5	216	444	520	655	69

<sup>a</sup>Glass transition temperature measured by DSC at a heating rate of 10°C/min in nitrogen.

<sup>b</sup>Temperature of onset of decomposition measured by TGA at a heating rate of 10°C/min in nitrogen.

<sup>c</sup>Temperature of maximum rate of weight loss measured by TGA at a heating rate of 10°C/min in nitrogen.

<sup>d</sup>Temperature of endset of decomposition measured by TGA at a heating rate of 10°C/min in nitrogen.

<sup>e</sup>Char yield at 800°C under nitrogen.

### 3.4: Morphological studies

The morphological studies of PEI/MBMI/ BaTiO<sub>3</sub> nanocomposite films were carried out using SEM. Figure 6 (a, b, c and d) shows the SEM micrographs of PM, PM1, PM3, PM5 semi-IPN and nanocomposites. It could be seen that BaTiO<sub>3</sub> particles were uniformly distributed throughout the PEI/MBMI semi-IPN system in lower wt% loading (1 and 3 wt%) however some agglomeration was observed in higher loading of the filler (5 wt%).

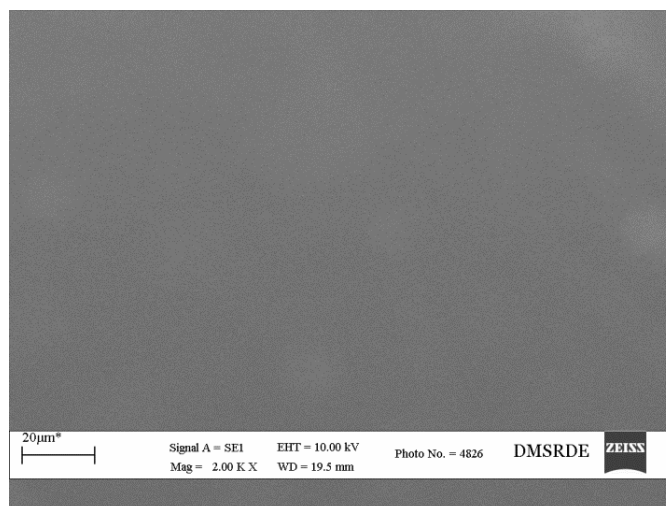


**Figure 6(a):** Scanning electron micrographs of PM.

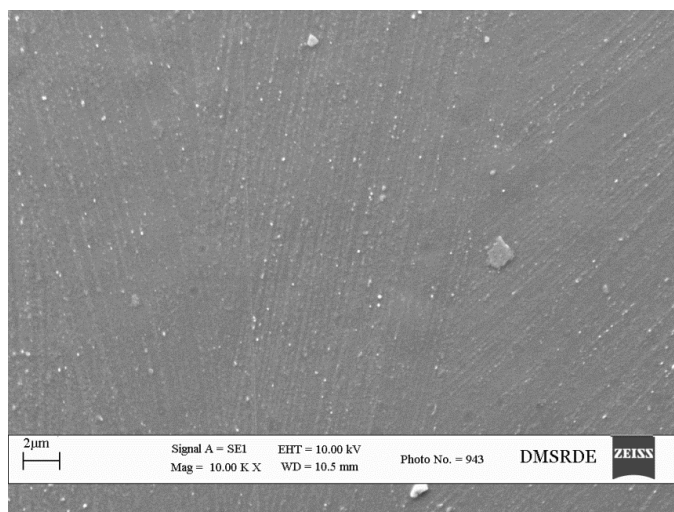


**Figure 6(b):** Scanning electron micrographs of PM1

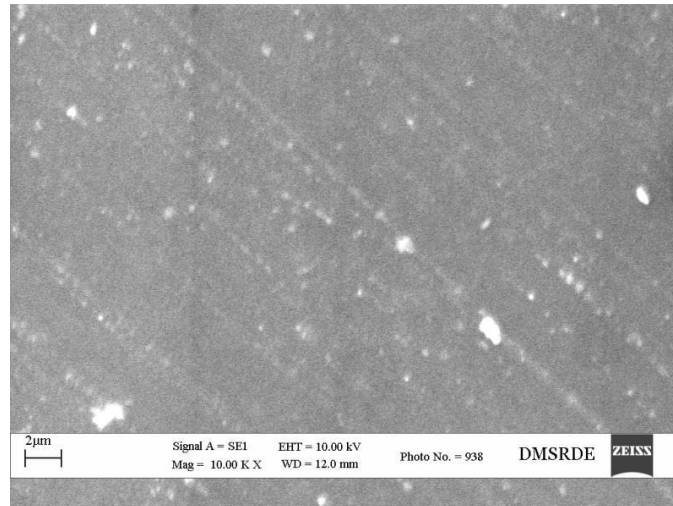


**Figure 6(c):** Scanning electron micrographs of PM3

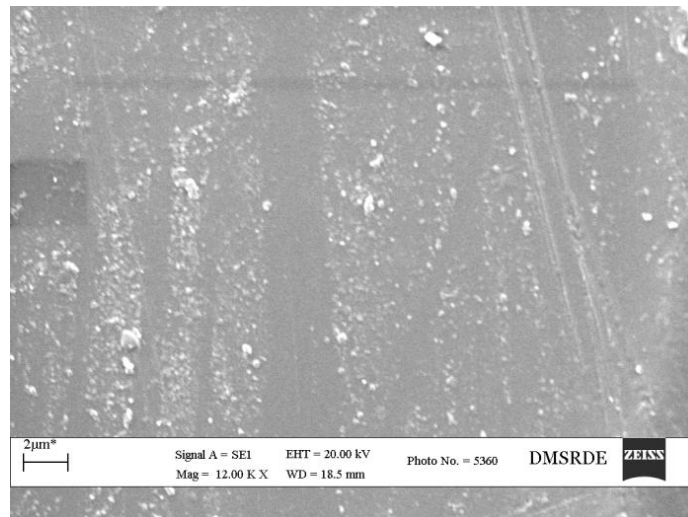


**Figure 6(d):** Scanning electron micrographs of PM5

### 3.5: Electrical Properties

Figure 7 and 8 show the effects of BaTiO<sub>3</sub> content on the dielectric constants and dielectric losses on PEI/MBMI/BaTiO<sub>3</sub> composite films at sweep frequencies of 10 kHz, 100 kHz and 1MHz. Dielectric constant values were calculated from the capacitance data using Eq 2

$$C = \frac{\epsilon_0 \epsilon_r A}{t} \quad \text{----- Eq 2}$$

Where,  $\epsilon_0$  is the dielectric permittivity of the free space ( $8.854 \times 10^{-12}$  F/m), A is the area of the electrical conductor, t is the thickness of insulating layer and  $\epsilon_r$  is the relative dielectric permittivity of the insulator layer. From Figure 7 and 8, it is clear that dielectric constant increases significantly with increasing BT content while the dielectric loss remains almost the same. For instance, the dielectric constant at sweep frequency of 10 kHz increases from 3.6 to 7.1 as BT content increases from 1 to 5 wt%, while the increase in loss is very less. This increase in the dielectric constant with increasing BT loading could be interpreted as due to increased interfacial polarization inside the composites in applied alternating field [28, 29]. This phenomenon appears in the heterogeneous system like ceramic-polymer composites due to accumulation of electric charges at the interface boundaries and the formation of large dipoles on ceramic particles or clusters. It is well known that the nanocomposites have a large volume fraction of interfaces which enhances the prospect of interfacial polarizations. This interfacial polarization has contributed to increased dielectric constant.

It can also be observed from Figure 7 that the dielectric constant values slightly come down with increasing frequency. The decreasing tendency of dielectric constant is thought to be a result of the dielectric relaxation of the BT nanoparticles at the interfaces in the nanocomposite [30]. At higher frequencies, there is insufficient time for relaxation and hence the contribution to polarizability decreases. This in turn decreases the dielectric constant at higher frequencies.

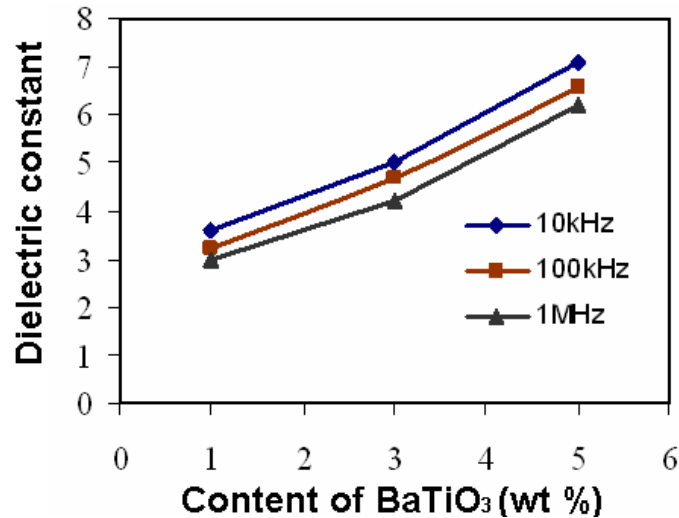


Figure 7: The effects of BaTiO<sub>3</sub> content on the dielectric constant of PEI/MBMI/BaTiO<sub>3</sub> nanocomposite.

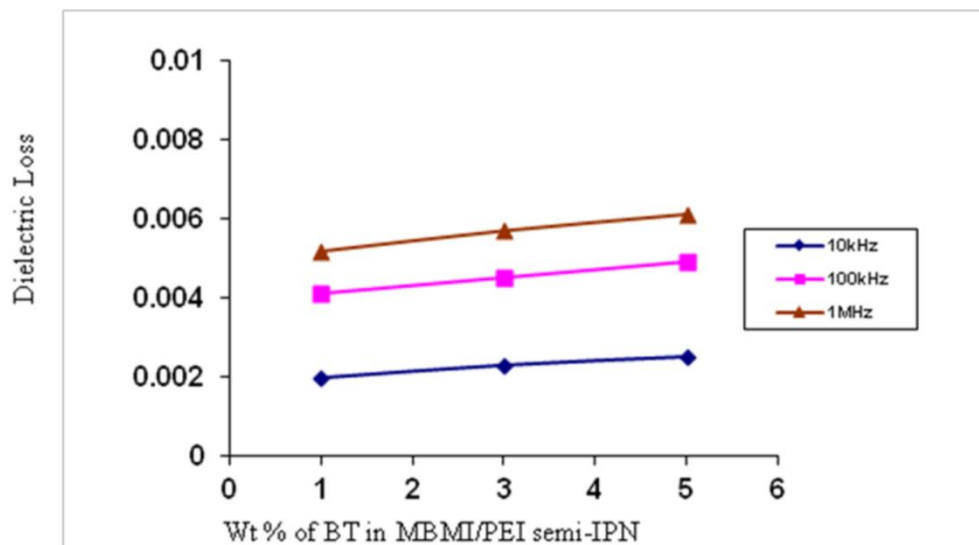


Figure 8: The effects of BaTiO<sub>3</sub> content on the dielectric losses of PEI/MBMI/BaTiO<sub>3</sub> nanocomposite.

### 3.6: Water Uptake

Water uptake of the PEI/MBMI semi-IPN and nanocomposite films was measured by immersing vacuum dried films into deionized water for 48h at room temperature. Then the films were taken out, wiped with tissue paper and quickly weighed on a microbalance. The water uptake of the films was calculated using the following equation

$$\text{Water Uptake (\%)} = \frac{W - W_0}{W_0} \times 100$$

Where,

$W_0$  is the initial weight of the polymer sample,  $W$  is the weight of the polymer sample after immersion in water for 48h. The amount of moisture uptake for these semi-IPN systems is shown in Figure 9. The data are an

average of three measurements with the error limit of 2%. Researchers have suspected that the water absorption is related to free volume in polymers [31-34]. From Figure 9, it is clear that as the content of BaTiO<sub>3</sub> increases in PEI/MBMI semi-IPN system water uptake decreases from 1.0 to 0.5. This decrease in water absorption is mainly associated with the reduction in free volume fraction in composite films.

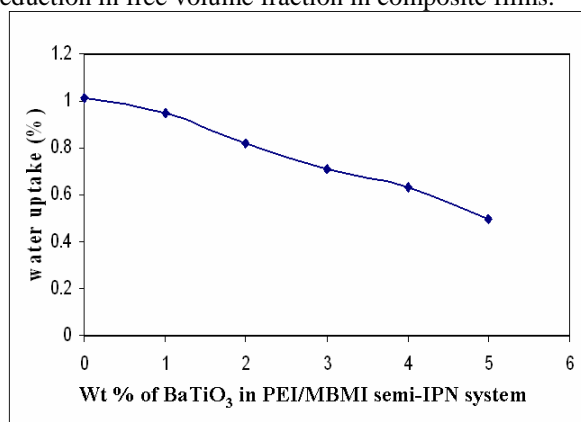


**Figure 9:** The effect of BaTiO<sub>3</sub> contents on the water uptake of PEI/MBMI/BaTiO<sub>3</sub> nanocomposite.

#### IV. CONCLUSIONS

PEI/MBMI/BT nanocomposite films were successfully prepared by in-situ polymerization method. The obtained nanocomposites possessed higher thermal stability than a neat PEI/MBMI semi-IPN matrix. With increasing wt% of BT nanoparticles the decomposition temperature of MBMI/PEI semi-IPN increased. It was found by SEM micrographs that BT nanoparticles were dispersed homogeneously in the PEI/MBMI semi-IPN matrix. The dielectric constant of PEI/MBMI/BT nanocomposite increases with increasing BT content. The author foresees that the nanocomposites reported herein may find applications as embedded capacitors, interlayer dielectrics and other related applications.

#### ACKNOWLEDGEMENT

The authors thank Director, DMSRDE, Kanpur, India for providing laboratory facilities and his kind support to carry out this work successfully.

#### REFERENCES

- [1]. Wang, C; Gong, Y; Cunning, B.V; Lee, S; Le, Q; Joshi, S.R; Science Advances, 2021, 7, 1-10.
- [2]. Kim, J.J; Brown, A.D; Bakis, C.E; Smith, E.C; Composite Science and Technology, 2021, 207, 108712.
- [3]. Wang, H.; Zhong, W.; Xu, P.; Du, Q. *Macromol. Mater. Eng.* 2004, 289, 793–799.
- [4]. Liu, L.; Lu, O.; Yin, J.; Qian, X.; Wang, W.; Zhu, Z.; Wang, Z.; *Mater. Mater. Sci. Eng.* 2002, C22, 61–65.
- [5]. Shimojima, A.; Umeda, N.; Kuroda, K. *Chem. Mater.* 2001, 13, 3610–3616.
- [6]. Wang, Z.; Pinnavaia, T.J. *Chem. Mater.* 1998, 10, 1820–1826.
- [7]. Gilman J. W.; Morgan A.B.; Harris R.H.; Trulove P.C.; Delong H.C.; Sutto, T.E. *Polym Mater Sci Eng* 2000, 83, 59.
- [8]. Wu, J.; Yang, S.; Gao, S.; Hu, A.; Liu, J.; Fan, L. *Eur. Polym. J.* 2005, 41, 73–81.
- [9]. Kim, Y.; Lee, W. K.; Cho, W. J.; Ha, C. S. *Polym. Int.* 1997, 43, 129–136.
- [10]. Kim, Y.; Kang, E.; Kwon, Y.S.; Cho, W. J.; Cho, C.; Chang, M.; Ree, M.; Chang, T.;
- [11]. Ha, C.S. *Synth. Metals* 1997, 85, 1399–1400.
- [12]. Xie, S.H.; Zhu, B.K.; Li, J.B.; Wei, X.Z.; Xu, Z. K. *Polym. Test.* 2004, 23, 797–801.
- [13]. Tong, Y.; Li, Y.; Vie, F.; Ding M. *Polym. Int.* 2000, 49, 1543–1547
- [14]. Zhu, Z. K.; Yang, Y.; Yin, J.; Qi, Z. N. *J. Appl. Polym. Sci.* 1999, 73, 2977–2984.
- [15]. Sperling, L. H., *Interpenetrating Polymer Networks and Related Materials*, Plenum Press, New York, 1981.
- [16]. Seo, J.; Jang, W.; Lee, S.; Han, H. *Polymer Degradation and Stability*, 2008, 93, 298-304.
- [17]. Lee, S.; Jng, W.; Choi, S.; Tharanikkarasu, K.; Shul, Y.; Han, H. *J Appl Polym Sci* 2007, 104, 2965-72.
- [18]. Saimani, S.; Kumar, A. *J Appl Polym Sci* 2008, 110, 3606-15.
- [19]. Pan, H.; Pu, H.; Wan, D.; Jin, M.; Chang, Z. *J of Power Sources* 2010, 195, 3077-83.
- [20]. Gupta, P.; Alam, S. *J. Appl. Polym. Sci.* 2011, 120, 2790-99.
- [21]. Varma, I. K.; Fohlen, G.M.; Parker J.A.; Frosch. R. A. U.S. Patent No. 4,276,344, 1981.
- [22]. Alexander D.C. U.S. Patent No. 4,876,358, 1989.
- [23]. Xing, X.; Deng, J.; Chen, J.; Liu, G. *Journal of Alloys and Compounds* 2004, 384, 312–317.
- [24]. Pant, H.C.; Patra, M.K.; Verma, A.; Vadera, S.R.; Kumar, N. *Acta Materialia* 2006, 54, 3163–3169.
- [25]. Harizanov, O.; Harizanova, A.; Ivanova, T. *Materials Science and Engineering B* 2004, 106, 191–195.
- [26]. Hara, M.; Sauer, J.A.; *Rev Macromol Chem Phys* 1994, C34, 325.
- [27]. Xing, P.; Robertson, G. P.; Guiver, M. D.; Mikhailenko, S. D.; Wang, K.; Kanliaguine, S. *J Membr Sci* 2004, 229, 95.
- [28]. Lozano, K.; Bonilla-Rios, J.; Barrera E. V. *J. Appl. Polym. Sci.* 2001, 79, 125-133.
- [29]. Rao, Y.; Qu, J.; Marinis, T.; Wong, C. P. *IEEE Trans Components Pack Technol* 2000, 23, 680–3. Vo, H. T.; Shi, F. G. *Microelectronics J.* 2002, 33, 409–15.
- [30]. Wang, S-F; Wang, Y-R.; Cheng, K-C.; Hsiao, Y-P. *Ceramic International* 2009, 35, 265-268.
- [31]. Lim, B. S.; Nowick, A. S.; Lee, K.-W.; Viehbeck, A. *J Polym Sci Part B; Polym*

- [32]. Phys 1993, 31, 545.
- [33]. Subrahmanyam, H. N.; Subrahmanyam, S. V. J Mater Sci 1987, 22, 2079.
- [34]. Tchangai, T.; Segai, Y.; Dukkali, K. J Appl Polym Sci 1989, 38, 305.
- [35]. Matsuguchi, M.; Sadaoka, Y.; Nasaka, K.; Ishibashi, M.; Kuroiwa, T.; Ito, A. J.
- [36]. Electrochem 1993, 140, 825.